Power estimation of flapping foil energy harvesters using vortex impulse theory

Firas F. Siala, James A. Liburdy*

Department of Mechanical Engineering, Oregon State University, Corvallis, OR 97331, USA

Abstract

This study explores the feasibility of using the vortex impulse approach, based on experimentally generated velocity fields to estimate the energy harvesting performance of a sinusoidally flapping foil. Phase-resolved, two-component particle image velocimetry measurements are conducted in a low-speed wind tunnel to capture the flow field surrounding the flapping foil at reduced frequencies of $k = fc/U_\infty = 0.06$ - 0.16, pitching amplitude of $\theta_0 = 70°$ and heaving amplitude of $h_0/c = 0.6$. The model results show that for the conditions tested, a maximum energy harvesting efficiency of 25% is attained near $k = 0.14$, agreeing very well with published numerical and experimental results in both accuracy and general trend. The vortex impulse method identifies key contributions to the transient power production from both linear and angular momentum effects. The efficiency reduction at larger values of reduced frequencies is shown to be a result of the reduced power output from the angular momentum. Further, the impulse formulation is decomposed into contributions from positive and negative vorticity in the flow and is used to better understand the fluid dynamic mechanisms responsible for producing a peak in energy harvesting performance at $k = 0.14$. At the larger k values, there is a reduction of the advective time scales of the leading edge vortex (LEV) formation. Consequently, the LEV that is shed during the previous half cycle interacts with the foil at the current half cycle resulting in a large negative pitching power due to the reversed direction of the kinematic motion. This vortex capture process significantly decreases the total cycle averaged power output and energy harvesting efficiency. These results show the link between the kinematic motion and LEV time scales that affect the overall power production.

Keywords: Flapping foil energy harvesters, leading edge vortex, impulse theory

1. Introduction

The rising global trend to reduce dependence on fossil fuels has provided significant motivation toward the development of alternative energy conversion methods and new technologies to improve their efficiency. Recently, flapping foil energy harvesters have been

*Corresponding author

Email address: james.liburdy@oregonstate.edu (James A. Liburdy)

gaining a wider scope of attention as a means of extracting energy from streams, rivers, tidal flows and wind [1]. These devices offer important advantages to the conventional rotary turbines from efficiency, economic and environmental perspectives [2]. For example, these systems can use significantly lower free stream velocities, allowing for a wider range of available resource sites at both large and small scales. Their operation can mitigate the occurrence of centrifugal stresses on the foil resulting in less structural constraints, as well as having reduced noise output and animal interactions [3].

The concept of flow energy harvesting using flapping foils was proposed by McKinney and DeLaurier [4]. The motion kinematics of the flapping foil, which is typically modeled as combined sinusoidal heaving and pitching motion at very large angles of attack, results in flow separation and formation of the leading edge vortices (LEVs). LEV structures produce regions of low-pressure on the suction side of the foil and generate a large suction force as long as they remain attached to the foil surface [5]. It is widely acknowledged that the LEV provides a mechanism for the high energy harvesting capabilities of flapping foils [1]. This is in contrast to the traditional wind/hydro-turbines, where the flow must remain attached to the foil surface to achieve high energy harvesting efficiency levels.

The vast majority of published studies on flapping foil energy harvesters have utilized numerical simulations to perform parametric investigations and to optimize the overall performance [3, 6–8]. The instantaneous power extracted by the flapping foil from the fluid flow is defined as follows:

$$P = F_y\dot{h} + M\dot{\theta} \tag{1}$$

where F_y is the force in the direction of heaving motion, $\dot{h}$ is the heaving velocity, M is the pitching moment and $\dot{\theta}$ is the pitching velocity. It has been shown that the rate of energy harvesting is maximized when operating at reduced frequencies of $k = fc/U_\infty = 0.10 - 0.15$ (where f is oscillation frequency, c is foil chord length and U_∞ is free stream velocity), heaving amplitudes of $h_0/c = 0.5 - 1.0$, pitching amplitudes of $\theta_0 = 70^\circ - 90^\circ$ and a phase shift of 90° between the heaving and pitching motions [3, 7, 9]. Currently, the majority of research studies on flapping energy harvesters are concerned with developing mechanisms to further enhance energy extraction capacity. Such mechanisms include the use of non-sinusoidal motion and structural flexibility of the foil [10–13]. These mechanisms, as well as others, attempt to control the LEV evolution to enhance the forces and their timing during the flapping cycle. Major contributions to understanding the complexities of LEVs have come from animal and insect flight [14–17]. However, energy harvesting typically occurs at relatively low reduced frequencies, where there is a dearth of knowledge concerning LEV evolution and mechanisms responsible for establishing the LEV time scales to compliment the much slower relative oscillation time scales of energy harvesting. Of particular interest is application of the optimal vortex formation by Gharib et al. [18]. Dabiri [19] has shown that there exists a strong correlation between the optimal vortex formation and thrust produced by swimming animals through vortex propulsion. However, it remains unknown whether this correlation also applies to LEV formation and energy harvesting efficiency of flapping foils. In addition to LEVs, operating at such low reduced frequencies may also trigger the formation of other large-scale flow structures such as trailing edge vortices (TEVs) [20].

To design more effective mechanisms of energy harvesting enhancement, there is a need to investigate the relationship between the dynamics of flow structures and power production in greater depth.

The relationship between flow structures and power production is typically studied qualitatively, where the vorticity field is synchronized with the instantaneous fluid dynamic force and moment [9, 21]. The disadvantage of this method is that it does not allow one to quantify the effects of different flow structures on the total force. In addition, it is often not feasible to experimentally measure the fluid dynamic forces accurately due to challenges in separating the inertial contributions from the total measured force [22]. This is especially a problem in wind tunnel experiments, where the foil density can be orders of magnitude greater than the density of air. As a result, wind tunnel experiments have been focused on very low reduced frequencies in order to minimize the inertial effects [23]. Recently, many authors began using the concept of vortex impulse to estimate the fluid dynamic forces from the measured velocity field [24–28]. Originally, this concept was introduced to bypass the integration of total momentum in infinite regions [29–31]. Estimating the fluid dynamic forces using the vortex impulse technique offers several advantages. For example, it only requires the knowledge of the velocity field, where the evaluation of pressure field is not required. This makes it a very attractive tool for the experimental fluid dynamics community since inferring the pressure field from velocity data is often a non-trivial task. In addition, since the impulse equation is linearly dependent on vorticity, it is possible to quantify the contribution of different vortex structures to the total force, which is quite advantageous when, for example, the goal is to design mechanisms that enhance the LEV contribution to force generation and power output.

The objectives of this paper are: (i) to explore the feasibility of using experimentally-generated velocity fields to estimate the energy harvesting performance and (ii) to better elucidate the mechanisms of power production of flapping foils. Two-component PIV measurements are conducted to capture the flow field surrounding the flapping foil. The aerodynamic loads and moment are determined using the finite-domain impulse theory [32]. While the impulse theory has been used extensively in estimating the lift and drag forces, to the best of our knowledge, its application for estimating the pitching moment has not been reported in the literature.

The rest of the paper is organized as follows. In Section 2, the details of experimental methodology are presented. In Section 3, the techniques of data analysis are provided. Section 4 presents results of lift and moment analysis and power production. Finally, conclusions and implications of this work are provided in Section 5.

2. Methodology

The experimental setup in the wind tunnel and a zoomed-in view of the motion device are sketched in Fig. 1. The foil was fabricated using fused deposition modeling, and has a chord length, thickness and aspect ratio of 125 mm, 6.25 mm and 2, respectively. The foil is attached to the motion device using a titanium rod spanning through the mid-chord of the foil. The motion device is used to generate the heaving and pitching motion according

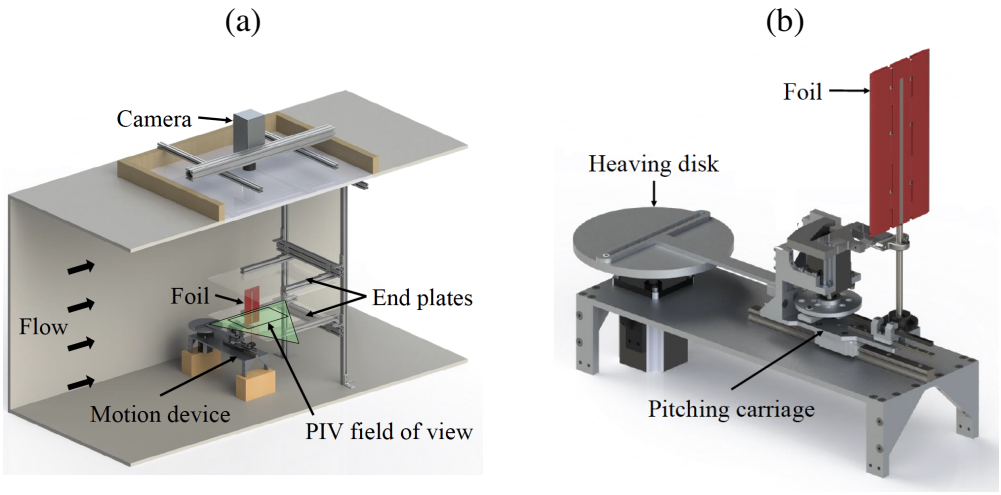

Figure 1: (a) Drawing of the experimental setup illustrating the wind tunnel, motion device and PIV system and (b) zoomed-in view of the motion device. Figures are adopted from [33].

to the following equations:

$$h(t) = h_0 cos(2\pi f t) \tag{2}$$

$$\theta(t) = \theta_0 cos(2\pi f t + \Phi) \tag{3}$$

where h_0 is the heaving amplitude, θ_0 is the pitching amplitude, Φ is phase shift between heaving and pitching and t is time. In this study, the heaving amplitude, pitching amplitude and phase shift are fixed at $h_0/c = 0.6$, $\theta_0 = 70°$ and $\Phi = 90°$, respectively, whereas the reduced frequency, k, was varied from 0.06 to 0.16 in increments of 0.02. A sketch of the foil motion is shown in Fig. 2(a). Furthermore, the motion kinematics can be integrated into the effective angle of attack, which is typically defined as follows:

$$\alpha_e = \theta(t) - arctan\left(\frac{\dot{h}(t)}{U_\infty}\right) \tag{4}$$

The effective angle of attack for one cycle is plotted in Fig. 2(b) for $k = 0.06 - 0.16$.

Phase-resolved particle image velocimetry measurements were conducted at the mid-span with a vector resolution of 1.8 mm (approximately 70 vectors per chord length). End plates were used to mitigate the three-dimensional effects. The phase-averaged velocity fields were obtained by averaging one hundred images at each phase of interest. A total of 116 phases during the downstroke motion with an equal spacing of $\Delta t/T = 0.004$ were acquired. To capture the entire flow field surrounding the oscillating foil, the experiments were repeated at a phase delay of 180° for each of the 116 phases. The 180° out of phase flow fields were then mirrored and stitched to the rest of the vector field to construct the full flow field surrounding the foil [34]. Uncertainty analysis based on the statistical-correlation technique developed by Wieneke [35] yielded an average uncertainty of 1.3% and 2.1% of the local stream-wise and cross-stream velocity component, respectively.

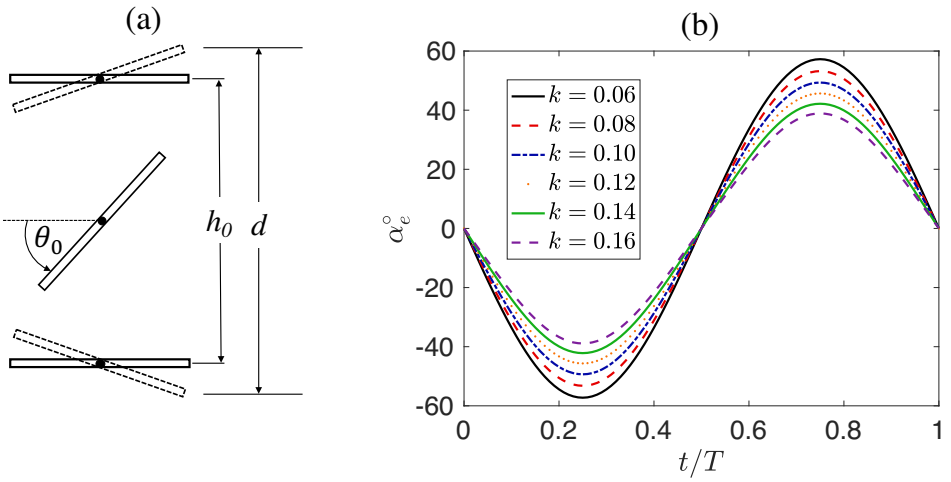

Figure 2: (a) Heaving and pitching motion. The foil pitching center is located at $c/2$ and d is the total crossflow distance swept by the foil. (b) Effective angle attack versus time for $k = 0.06$-0.16

3. Data analysis

The total cycle-averaged power coefficient is divided into two components, the power from heaving motion $\overline{C_{P,h}}$ and the power from pitching motion $\overline{C_{P,\theta}}$:

$$\overline{C_P} = \overline{C_{P,h}} + \overline{C_{P,\theta}} \tag{5}$$

where the cycle-averaged heaving and pitching power coefficients are defined as follows:

$$\overline{C_{P,h}} = \frac{2\overline{F_y \dot{h}}}{\rho U_\infty^3 c} \tag{6}$$

$$\overline{C_{P,\theta}} = \frac{2\overline{M_z \dot{\theta}}}{\rho U_\infty^3 c} \tag{7}$$

Furthermore, we define the energy harvesting efficiency, η, as the ratio of power output to the available fluid power in the swept area of the two dimensional foil. Similar to the power coefficient, the total efficiency is decomposed into heaving and pitching components such as follows:

$$\eta_h = \overline{C_{P,h}} \frac{c}{d} \tag{8}$$

$$\eta_\theta = \overline{C_{P,\theta}} \frac{c}{d} \tag{9}$$

where d is the total crossflow length swept by the foil.

The two-dimensional impulse-based aerodynamic force [32] can be written as follows:

$$\mathbf{F} = -\rho\frac{d}{dt}\int_A \mathbf{x}\times\boldsymbol{\omega}dA + \rho\int \mathbf{u}\times\boldsymbol{\omega}dA - \rho\oint_S \mathbf{n}\cdot\Big([\mathbf{u}(\mathbf{x}\times\boldsymbol{\omega})]\Big)dS + \oint_S [\mathbf{x}\cdot(\nabla\cdot\mathbf{T})\mathbf{I} - \mathbf{x}(\nabla\cdot\mathbf{T})]dS + \mathbf{F}_{AM} \quad (10)$$

where $\mathbf{x}$ is the position vector, $\boldsymbol{\omega}$ is the vorticity vector, $\mathbf{u}$ is the velocity vector, $\mathbf{T}$ is the stress tensor, $\mathbf{I}$ is the identity tensor and $\mathbf{n}$ is the normal vector. The first term is integrated over the fluidic area A that is bounded by the control volume surface S and the foil surface, where as the second, third and fourth terms are integrated over the control volume surface S. Although the equation above is theoretically independent of the origin location $\mathbf{x}_0$, Siala [34] has shown that by choosing an origin located on the downstream boundary of the control volume, the surface integrals can be shown to have negligible contributions, and the two-dimensional force equation can be written as follows:

$$\mathbf{F} = -\rho\frac{d}{dt}\int \mathbf{x}\times\boldsymbol{\omega}dA + \rho\int \mathbf{u}\times\boldsymbol{\omega}dA + \mathbf{F}_{AM} \quad (11)$$

The advantage of this simplified equation is that it contains only three terms with clear physical meaning. The first term on the right-hand side is referred to as the impulse force and it is associated with the growth and advection of vortical structures in the control volume [36]. The second term on the right-hand side is referred to as the vortex force, which represents the effect of vortex structures outside of the control volume on the total force [27, 34]. The term F_{AM} is the added-mass force, which represents the force felt by the oscillating foil as it pushes against the adjacent fluid. For thin foils submerged in air, the added-mass force is negligible.

The aerodynamic moment equation (derived in [34]) can be shown to be written as follows:

$$\mathbf{M} = \rho\frac{1}{2}\frac{d}{dt}\int x^2\boldsymbol{\omega}dA - \rho\int \mathbf{x}\times(\mathbf{u}\times\boldsymbol{\omega})dA - \rho\frac{1}{2}\oint x^2\mathbf{n}\times(\mathbf{u}\times\boldsymbol{\omega})dS \quad (12)$$

where we refer to the first and second terms on the right-hand side as the impulse moment and vortex moment, respectively. The third term on the right-hand side takes into account the contributions of flow structures passing through the boundary (S) of the control volume. The errors from the velocity fields were propagated to the force and moment in order to calculate their uncertainty, which were estimated to be 13.6% and 16.2% of their maximum value, respectively.

One important advantage of the impulse-based force and moment equations is that they are linearly dependent on vorticity, meaning that total force and moment impulse can be treated as a superposition of impulses of every individual vortex structure in the flow. For simplicity, in this study we categorize two different vortical structures: one with positive sign vorticity, and the other with negative sign vorticity. We define the heaving power coefficient of the positive vortical structures noted with "+" as:

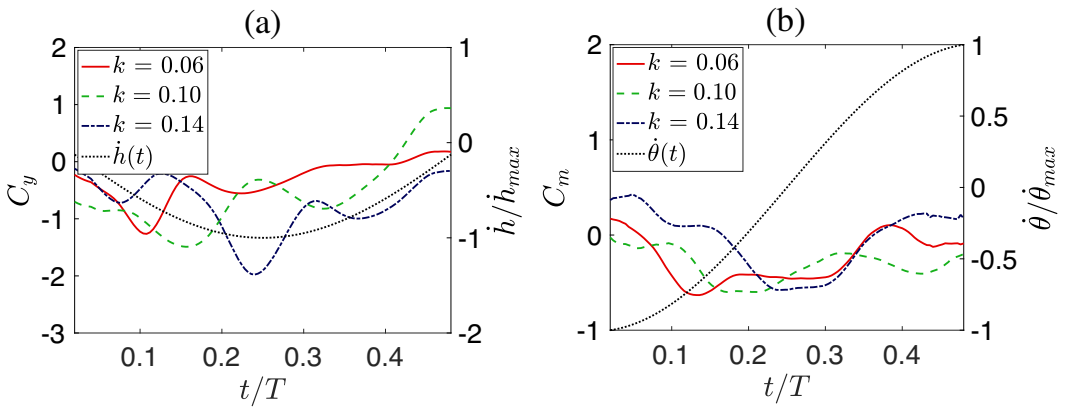

Figure 3: (a) Coefficient of lift and heaving velocity and (b) coefficient of moment and pitching velocity, for $k = 0.6$, 0.10 and 0.14.

$$C_{P,h^+} = \frac{2F_{y^+}\dot{h}}{\rho U_\infty^3 c} \tag{13}$$

$$C_{P,\theta^+} = \frac{2M_{z^+}\dot{h}}{\rho U_\infty^3 c} \tag{14}$$

Similarly, the pitching power coefficient of the negative vortical structures noted with "-" as:

$$C_{P,h^-} = \frac{2F_{y^-}\dot{h}}{\rho U_\infty^3 c} \tag{15}$$

$$C_{P,\theta^-} = \frac{2M_{z^-}\dot{h}}{\rho U_\infty^3 c} \tag{16}$$

Upon analyzing the power production using the above decomposition, one can correlate the vorticity dynamics with the performance more effectively.

4. Results

The results of this study determine the overall power production performance based on both efficiency and power coefficient. Experimentally measured velocity fields are used to evaluate the unsteady aerodynamic lift and moment during the cycle with results given here for the downstroke motion. The upstroke motion results are a repetition of the downstroke with associated sign reversal. Velocity data are used to identify the dominant flow structures as they relate to the power production.

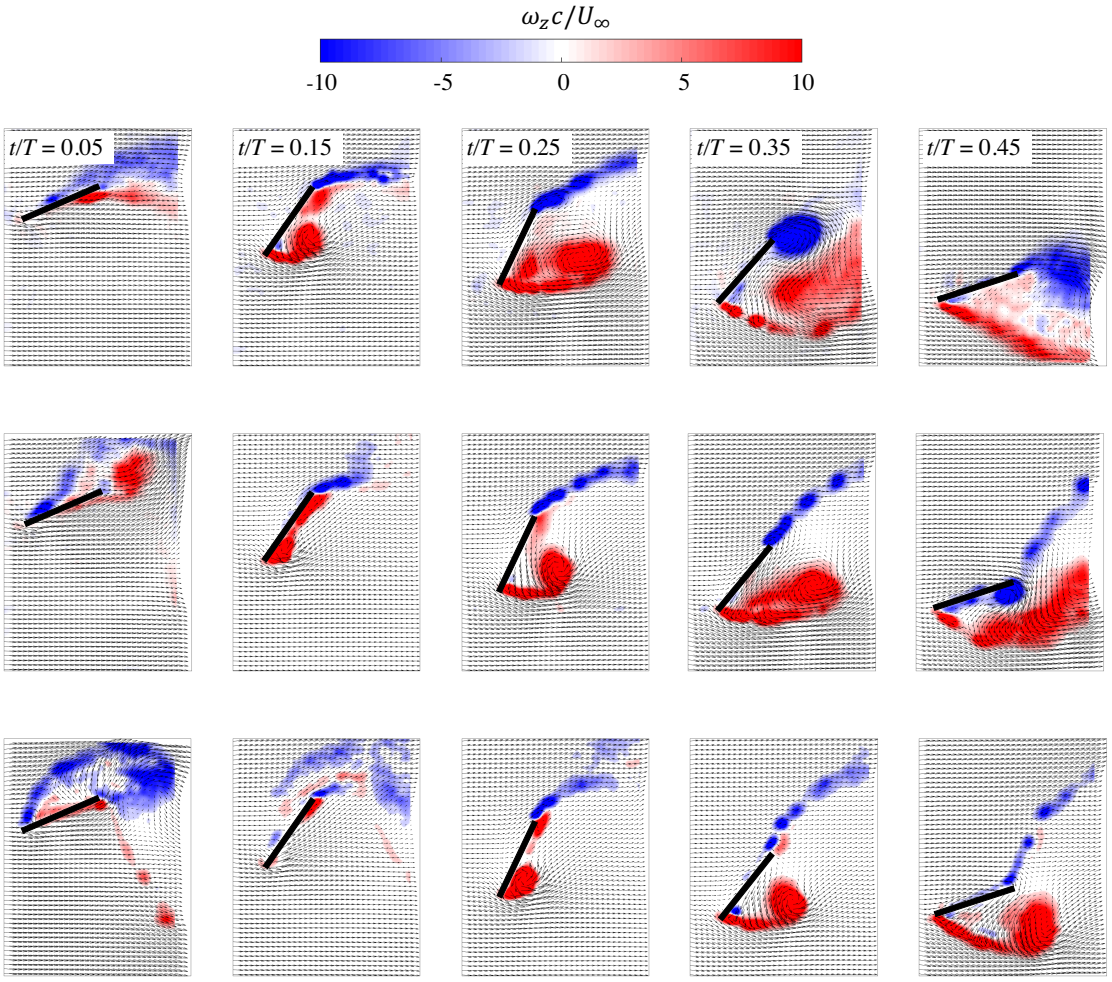

Figure 4: Phase-averaged vorticity field for discrete phases during the downstroke. Top row: $k = 0.06$, middle row: $k = 0.10$ and bottom row: $k = 0.14$. For clarity, only every fourth vector is plotted.

4.1. Force and moment estimation

The transient force ($C_y = 2F_y/\rho U_\infty^2 c$) and moment ($C_m = 2M_z/\rho U_\infty^2 c^2$) coefficients are plotted in Fig. 3(a) and 3(b), respectively, for $k = 0.06$, 0.10 and 0.14. The heaving and pitching velocities are also included. The force coefficient experiences an initial dominant peak followed by a secondary peak. Note that for $k = 0.14$, there is also a preliminary smaller peak that occurs early in the cycle at $t/T \approx 0.05$. The timing of the dominant peak events is shown to delay to later times in the cycle as the reduced frequency increases. Also, increasing the reduced frequency increases the magnitude of this peak force. In contrast, increasing the reduced frequency has minimal influence on the magnitude of the peak moment coefficient, but it does delay the occurrence of the peak to later times in the cycle. The phase shift of the force and moment coefficients can be understood by analyzing the spatio-temporal evolution of vortical structures in the flow.

In Fig. 4, we show the evolution of the phase-averaged vorticity and velocity fields for $k = 0.06$, 0.10 and 0.14. The flow approaches from the left and the non-dimensional time $t/T = 0$ corresponds to the top heaving position. It is quite obvious that the inception of the LEV is delayed when the reduced frequency increases. This is associated with the decrease in the foil oscillation time scale relative to the flow time scale. As a result, the shear layer requires a longer time to react to the change in the geometric angle of attack as k increases, thereby delaying separation. The timing of peak force generation coincides with the time at which the LEV is lifted-off the foil surface, whereas the peak moment occurs slightly later. The peak moment has negative values, indicating that when the LEV forms on the bottom surface of the foil, it creates a downward force on upstream portion of the foil. This induces a counter-clockwise moment about the pitching axis (mid-chord). The magnitude of moment coefficient begins to decrease once the LEV advects downstream beyond the foil center. Subsequently, the trailing edge shear layer rolls-up into a TEV when the LEV approaches the foil trailing edge when $k = 0.06$ and 0.10. For $k = 0.06$, the formation of the TEV ($t/T \approx 0.25$) results in only a slight decrease in the force coefficient, whereas its influence on the moment coefficient is negligible. This is because the TEV advects downstream into the wake shortly after it forms, such that its influence on the foil is not significant. On the other hand for $k = 0.1$, the TEV is shown to completely roll on the bottom surface of the foil by the end of the downstroke motion. Consequently, its influence on the foil is more profound, which is reflected by the rapid decrease in the force and increase in counter-clock wise moment at $t/T \approx 0.4$.

By increasing the reduced frequency to $k = 0.14$, the advective time scale of the flow becomes even longer relative to the oscillation time scale. This results in the LEV that is shed during the previous upstroke to remain near the foil trailing edge as the foil begins its downward motion ($t/T \approx 0.05$). The foil takes advantage of the proximity of this LEV to produce an early small downward force peak, as is shown in Fig. 3(a). In addition, as the newly formed LEV approaches the foil trailing edge at $t/T = 0.45$, it is observed that the trailing edge vortex sheet does not roll-up into a large TEV. This is because the LEV approaches the trailing edge rather late in the cycle when the geometric angle of attack is relatively small. As a consequence, the trailing edge shear layer does not roll into a large vortex.

4.2. Power output

The total instantaneous power coefficient is shown in Fig. 5, along with the heaving and pitching contributions for $k = 0.06$, 0.10 and 0.14. For $k = 0.06$, the total power coefficient (C_P) has three distinct peaks. The first peak is produced at $t/T \approx 0.12$, where both the heaving and pitching motions have a comparable contribution. At this instant, the LEV has just lifted-off the surface of the foil, which results in peak force and moment coefficients as shown in Fig. 3. The peak force and moment coefficients both have the same sign as the heaving and pitching velocities, respectively, resulting in a positive power output. Furthermore, there is a secondary peak of C_P that occurs at $t/T \approx 0.22$, due to the heaving power ($C_{P,h}$). The timing of the secondary peak in $C_{P,h}$ coincides with the timing of the secondary force peak in Fig. 3. Siala [34] has shown that the secondary peak is

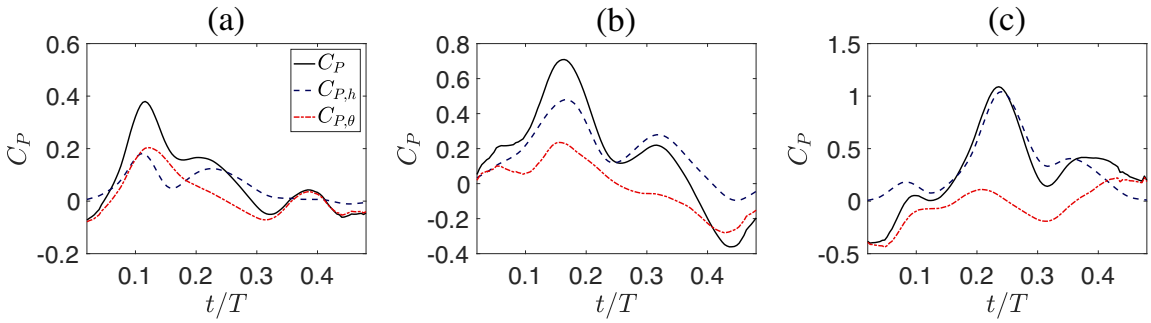

Figure 5: Transient power coefficient for (a) $k = 0.06$, (b) $k = 0.10$ and (c) $k = 0.14$.

strongly dependent on the enhanced LEV advection velocity. Finally, the third minor peak that occurs at $t/T \approx 0.38$ is associated with only the pitching power ($C_{P,\theta}$). At this time, a small positive (clock-wise) moment peak is generated that has the same sign as the pitching velocity (which is undergoing a pitching reversal beyond $t/T = 0.25$), thereby producing a positive power output. As k is increased to 0.10, the timing of primary power peak is delayed to $t/T \approx 0.16$, which is a consequence of the delay in peak force generation with increasing reduced frequency. As shown, the heaving motion plays a more dominant role in this peak power than the pitching motion. A key difference between $k = 0.10$ and $k = 0.06$ is that the pitching motion produces considerable negative power in the second half of the downstroke. As discussed above, the TEV for this higher reduced frequency remains in close proximity to the bottom surface of the foil, which results in a relatively large negative moment. Therefore, the product of the negative moment and positive pitching velocity of the foil is negative. Increasing k further to 0.14 the total power is shown to have relatively large negative values at the beginning of the downstroke due to the pitching contribution. This is a result of the LEV being shed from the previous upstroke half cycle that is captured by the foil as it begins its downstroke (see Fig. 4). In this case, the clock-wise rotating LEV that is advecting near the foil trailing edge along the upper surface generates a large positive moment about the pitching axis, which interacts with counter-clockwise rotating foil to produce a negative power output. At this higher reduced frequency, the pitching power has a negligible contribution to the primary power peak, which is generated at $t/T \approx 0.23$. Although the moment coefficient at this time is maximum, the foil is about to reverse its pitching motion from counter clock-wise to clock-wise rotation, such that the pitching velocity approaches zero (hence $C_{P,\theta} \approx 0$). Beyond $t/T \approx 0.25$ the pitching velocity switches sign from negative to positive, whereas the moment coefficient remains to be negative for a short period beyond this time and thus the product of the two results in a negative pitching power. Eventually, the LEV advects pasts the foil mid-chord and a small positive pitching power is produced at $t/T > 0.4$.

The total, heaving and pitching energy harvesting efficiency are shown in Fig. 6(a). As shown, the total energy harvesting efficiency (η) increases with increasing reduced frequency until a maximum of approximately 25% is attained at $k = 0.14$. Beyond $k = 0.14$, the

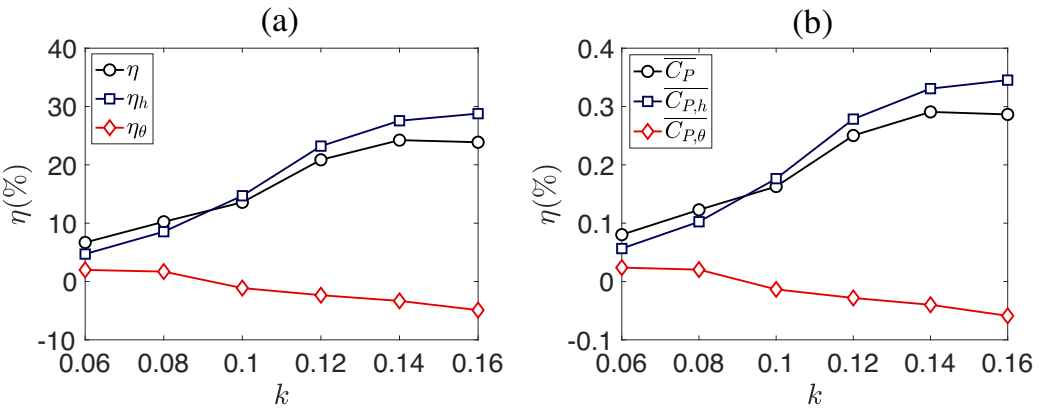

Figure 6: (a) Energy harvesting efficiency and (b) mean power coefficient. The individual contributions of the heaving and pitching motions are also shown.

efficiency begins to decrease. The trend and efficiency values agree very well with other results reported in the literature [7]. For example, Zhu [3] obtained peak efficiency values of 25% - 30% at $k \approx 0.14$ for a wide range of heaving and pitching amplitudes. Furthermore for the range of reduced frequencies that we tested, the heaving efficiency (η_h) is shown to increase with increasing k, but the rate of increase begins to decrease at $k \geq 0.12$. On the other hand, the pitching efficiency (η_θ) contributes positively to the total energy harvesting efficiency for $k \leq 0.1$, which then begins to have a negative influence for $k > 0.1$. At $k = 0.16$, the pitching efficiency becomes large enough (negatively) such that the total energy harvesting efficiency begins to drop. This trend was also observed by Kim et al. [9]. The mean total power coefficient, as well as the heaving and pitching contributions are given in Fig. 6(b). The mean power coefficient and energy harvesting efficiency show the same trend, but they differ by a constant factor of c/d for the parameters studied here. The effects of changing c/d on the efficiency by altering the maximum pitching angle are discussed by Totpal et al. [23].

4.3. Optimal leading edge vortex formation

Based on the significant role of the LEV formation, we now investigate the relationship between the optimal vortex formation and energy harvesting efficiency. In Fig. 7(a), the non-dimensional LEV circulation is given as a function of time for $k = 0.06 - 0.16$. The circulation is normalized by the chord length and mean leading edge shear layer velocity. The latter is approximated using the flow velocity using a frame of reference at the foil leading edge tip [34, 37]. Note that this normalization of the LEV is consistent with the optimal vortex formation number parameter given by Dabiri [19]. The LEV circulation is computed based on the vortex identification technique proposed by Graftieaux et al. [38]. In this method, a scalar function, Γ_2, derived from the velocity vector field is used to identify the vortex boundary. The circulation is calculated by integrating the vorticity contained within the LEV boundary defined by $\Gamma_2 = 2/\pi$. It is shown in Fig. 7 that for $k \leq 0.10$, the

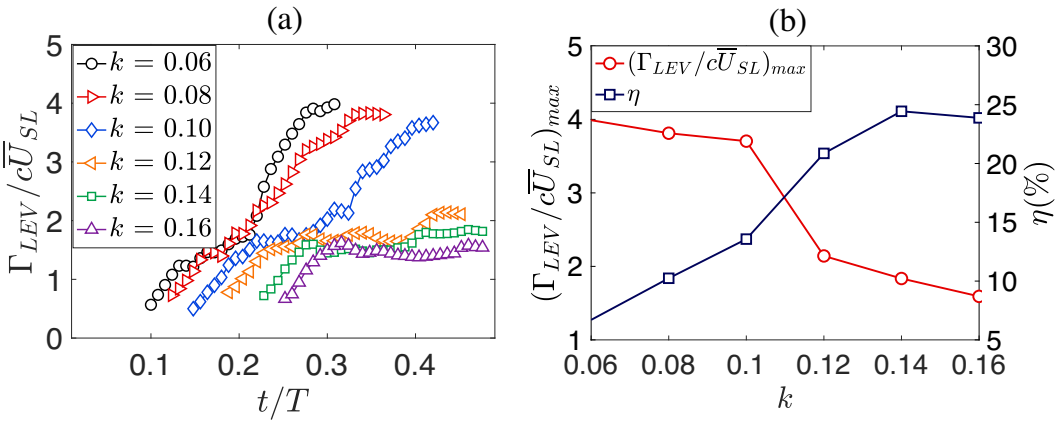

Figure 7: (a) Normalized LEV circulation versus time for $k = 0.06 - 0.16$ and (b) maximum LEV circulation and energy harvesting efficiency versus reduced frequency.

maximum LEV circulation falls within $3.8 - 4.0$, which is remarkably close to the universal optimal vortex formation number [18]. At these reduced frequencies the time scale of LEV growth is relatively small when compared to the oscillation time scale. This allows the LEV to grow to its maximum possible size (as is determined by the chord length) and circulation. This is reflected by the formation of the TEV at these reduced frequencies, which allows the LEV to grow past the trailing edge, thereby forcing the trailing edge shear layer to roll into a large vortex. When k is larger than 0.10, the time scale of the LEV growth is slow compared with the foil oscillation time scale such that the end of a cycle is reached before the LEV attains its maximum possible size and strength. Shown in Fig. 7(b) is the maximum vortex formation number obtained by the LEV and the energy harvesting efficiency as a function of reduced frequency. Clearly the efficiency increases while the LEV formation number decreases. But this negative correlation appears to be driven by the ratio of time scales that influence LEV formation relative to the foil kinematic time scale. The maximum efficiency occurs at $k = 0.14$, where the LEV formation number is approximately equal to 2. Unlike in propulsion applications where the optimal vortex formation in the near-wake results in the greatest thrust, flapping energy harvesting systems rely more on the timing of the LEV formation and detachment. The reduced frequency of $k = 0.14$ seems to result in the best match between the LEV flow and foil oscillation time scales.

4.4. Contribution of flow structures to power production

To further elucidate the mechanisms responsible for producing the peak in both the power coefficient and energy harvesting efficiency near $k = 0.14$, we investigate the power output using the decomposition proposed in Section 3. In Fig. 8, we show the the heaving power contribution from the positive, C_{P,h^+} and negative ,C_{P,h^-}, vorticity for $k = 0.10$, 0.14 and 0.16. It is quite evident that for all reduced frequencies, the power production is dominated by the positive vorticity in the flow (i.e. leading edge vortex and its feeding sheer layer). As discussed previously, the peak in the heaving power is due to formation of

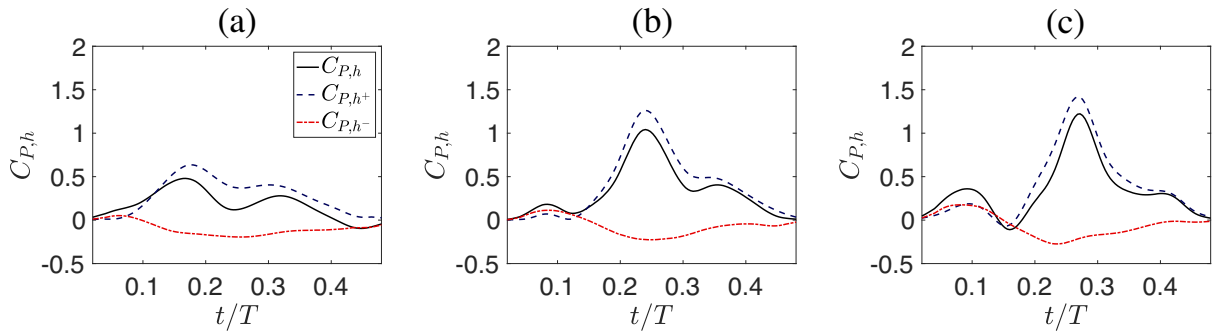

Figure 8: Transient heaving power coefficient showing the contributions of positive and negative vorticity for (a) $k = 0.10$, (b) $k = 0.14$ and (b) $k = 0.16$.

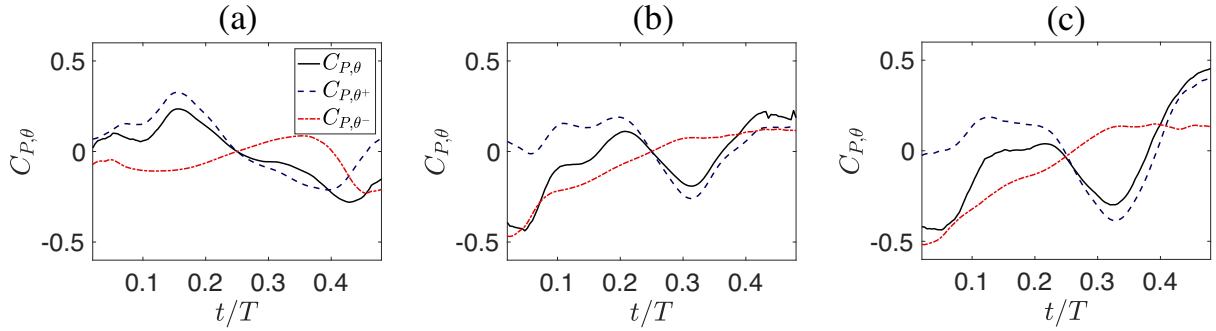

Figure 9: Transient pitching power coefficient showing the contributions of positive and negative vorticity for (a) $k = 0.10$, (b) $k = 0.14$ and (b) $k = 0.16$.

the LEV. Furthermore, the heaving power from the negative vorticity has a negative global maximum that occurs at $t/T \approx 0.25$. This is coincident with the time at which the heaving velocity is maximum. Note that the large TEV for $k = 0.10$ that forms at $t/T \approx 0.45$ (see Fig. 4) has a negligible contributions to heaving power production, since the heaving velocity of the foil at this phase of the cycle is small.

In Fig. 9, the contributions of the positive and negative vorticity to the pitching power coefficient are presented. As shown, the trend in the total pitching power is significantly different for $k = 0.10$ when compared to $k = 0.14$ and 0.16. The difference is dominated by the contribution of negative vorticity, C_{P,θ^-}. For $k = 0.14$ and 0.16, there is a negative pitching power due to negative vorticity at the beginning of the downstroke. This is a consequence of the LEV from the upstroke being "caught" by the foil as it begins pitching downward. This effect is intensified as k increases from 0.14 to 0.16. For $k = 0.10$, C_{P,θ^-} remains quite small until the TEV formation that occurs towards the end of the cycle (approaching the top heaving position) begins to produce relatively large negative pitching power. Furthermore, the positive vorticity contribution also has some distinct differences when comparing $k = 0.10$ to $k = 0.14$ and 0.16. For $k = 0.10$, there is a peak in C_{P,θ^+} that

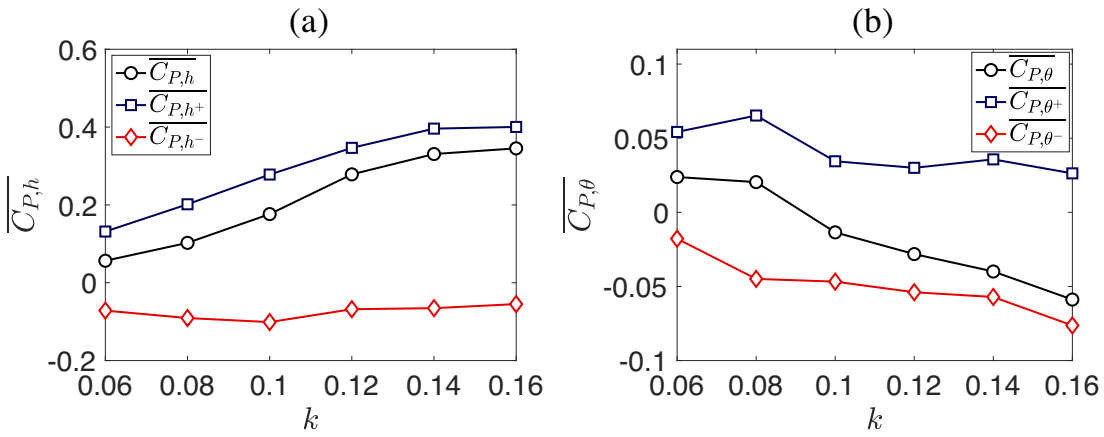

Figure 10: Cycle-averaged power contributions of the positive and negative vorticity to the (a) heaving power and (b) pitching power.

occurs at $t/T \approx 0.16$, which is due to the counter-clock wise moment produced by the LEV. This peak becomes less pronounced at the higher k values, since the LEV formation is shifted towards the mid-stroke, and consequently, the product of moment and pitching velocity is smaller (pitching velocity is zero at the mid-stroke). The large negative peaks of C_{P,θ^-} for $k = 0.14$ and 0.16 that occur at $t/T \approx 0.31$ and $t/T \approx 0.34$, respectively, are produced by the LEV that are still positioned in the up-stream portion of the foil. The negative counter clock-wise moment produced by the LEV is multiplied by the positive pitching velocity of the clock-wise rotating foil, thus producing negative power.

The cycle averaged power coefficient is shown in Fig. 10 for both the heaving and pitching contributions. Each is decomposed into contributions from positive and negative vorticty as indicated with the "+" and "-" signs. The negative vorticity contributes negatively to the total heaving power at an approximately constant value of $\overline{C_{P,h^-}} = 0.01$ for all reduced frequencies. On the other hand, the positive vorticity always has a favorable contribution, mainly due to the effects of the LEV. The mean contributions of the positive and negative vorticity on the pitching power is shown in Fig. 10(b). The negative vorticity is primarily responsible for the significant increase in negative pitching power production. For $k \leq 0.10$ this negative vorticity is due to the formation of the TEV structure near the end of the down-stroke. Whereas for $k \geq 0.10$ the LEV from the up-stroke is "caught" by the foil during the start of the downward pitching/heave motion and is the primary source of the negative pitching power.

Conclusions

Two dimensional particle image velocimetry experiments were conducted in a low-speed wind tunnel to investigate the feasibility of estimating the energy harvesting capabilities of a sinusoidally flapping foil energy harvesters using the impulse theory. The reduced frequency was varied from $k = 0.06$ to $k = 0.16$, and the pitching and heaving amplitudes

were set at $\theta_0 = 70°$ and $h_0/c = 0.6$, respectively. These results help to identify the relative contributions to power production caused by the dominant flow structures.

The impulse-based aerodynamic force and moment equations were shown to be consistent with other studies in estimating the power produced by the heaving and pitching motions, respectively. The maximum energy harvesting efficiency of approximately 25% was obtained at $k = 0.14$, agreeing very well with results reported in the literature for these conditions. The relationship between the concept of optimal vortex formation number and maximum energy harvesting efficiency was explored. The results show no established relationship between these two, and the maximum energy harvesting efficiency obtained at $k = 0.14$ is shown to be a result of the optimal match between the LEV and foil oscillation time scales.

In order to better understand the trends of energy harvesting efficiency and mean power output, the power production due to the lift force and torque were decomposed into contributions of positive and negative vorticity in the flow. It was observed that the contribution of the negative vorticity to the pitching motion was primarily responsible for the reduction of the harvesting efficiency and power output for $k > 0.14$. Specifically, due to the slower advective time scale of the LEV at higher k values, the clockwise rotating LEV generated during the previous cycle upstroke motion was shown to be caught by the downstream potion of the foil as it begins pitching/heaving downward. As a result, a large counter clockwise (negative) moment is produced, which interacts with the clock-wise rotating foil to produce a large negative pitching power.

The results of this study show that the impulse-based force calculation provides a means of investigating the mechanisms of power production of flapping energy harvesters in greater depth and detail. Future work will focus on further decomposing the impulse equations into vortex growth and vortex advection components. This may be of great importance to guide future studies in developing more effective kinematic motion in LEV-based energy harvesting systems.

Acknowledgment

The authors would like to thank Ali Mousavian and Cameron Planck for helping with designing the heaving/pitching device and developing the LabView code. Firas Siala acknowledges the financial support from Link Energy Foundation Fellowship. Also, financial support was provided from the Air Force Office of Scientific Research under the MURI grant FA9550-07-1-0540 and the National Science Foundation CBET Award Number 1804964.

References

[1] Q. Xiao, Q. Zhu, A review on flow energy harvesters based on flapping foils, Journal of Fluids and Structures 46 (2014) 174–191.

[2] J. Young, J. C. Lai, M. F. Platzer, A review of progress and challenges in flapping foil power generation, Progress in Aerospace Sciences 67 (2014) 2–28.

[3] Q. Zhu, Optimal frequency for flow energy harvesting of a flapping foil, Journal of Fluid Mechanics 675 (2011) 495–517.

[4] W. McKinney, J. DeLaurier, Wingmill: an oscillating-wing windmill, Journal of Energy 5 (2) (1981) 109–115.
[5] E. C. Polhamus, Predictions of vortex-lift characteristics by a leading-edge suctionanalogy, Journal of aircraft 8 (4) (1971) 193–199.
[6] G. Dumas, T. Kinsey, Eulerian simulations of oscillating airfoils in power extraction regime, WIT Transactions on Engineering Sciences 52.
[7] T. Kinsey, G. Dumas, Parametric study of an oscillating airfoil in a power-extraction regime, AIAA Journal 46 (6) (2008) 1318–1330.
[8] Z. Peng, Q. Zhu, Energy harvesting through flow-induced oscillations of a foil, Physics of fluids 21 (12) (2009) 123602.
[9] D. Kim, B. Strom, S. Mandre, K. Breuer, Energy harvesting performance and flow structure of an oscillating hydrofoil with finite span, Journal of Fluids and Structures 70 (2017) 314–326.
[10] Q. Xiao, W. Liao, S. Yang, Y. Peng, How motion trajectory affects energy extraction performance of a biomimic energy generator with an oscillating foil?, Renewable energy 37 (1) (2012) 61–75.
[11] W. Liu, Q. Xiao, F. Cheng, A bio-inspired study on tidal energy extraction with flexible flapping wings, Bioinspiration & biomimetics 8 (3) (2013) 036011.
[12] K. Lu, Y. Xie, D. Zhang, Nonsinusoidal motion effects on energy extraction performance of a flapping foil, Renewable Energy 64 (2014) 283–293.
[13] F. Siala, J. A. Liburdy, Energy harvesting of a heaving and forward pitching wing with a passively actuated trailing edge, Journal of Fluids and Structures 57 (2015) 1–14.
[14] J. G. Leishman, Unsteady lift of a flapped airfoil by indicial concepts, Journal of Aircraft 31 (2) (1994) 288–297.
[15] C. P. Ellington, C. Van Den Berg, A. P. Willmott, A. L. Thomas, Leading-edge vortices in insect flight, Nature 384 (6610) (1996) 626.
[16] R. Madangopal, Z. A. Khan, S. K. Agrawal, Biologically inspired design of small flapping wing air vehicles using four-bar mechanisms and quasi-steady aerodynamics, Journal of Mechanical Design 127 (4) (2005) 809–816.
[17] M. F. Platzer, K. D. Jones, J. Young, J. S. Lai, Flapping wing aerodynamics: progress and challenges, AIAA Journal 46 (9) (2008) 2136–2149.
[18] M. Gharib, E. Rambod, K. Shariff, A universal time scale for vortex ring formation, Journal of Fluid Mechanics 360 (1998) 121–140.
[19] J. O. Dabiri, Optimal vortex formation as a unifying principle in biological propulsion, Annual Review of Fluid Mechanics 41 (2009) 17–33.
[20] F. F. Siala, A. D. Totpal, J. A. Liburdy, Optimal leading edge vortex formation of a flapping foil in energy harvesting regime, in: ASME 2017 Fluids Engineering Division Summer Meeting, American Society of Mechanical Engineers, 2017, pp. V01CT23A008–V01CT23A008.
[21] Y. Xie, K. Lu, D. Zhang, Investigation on energy extraction performance of an oscillating foil with modified flapping motion, Renewable Energy 63 (2014) 550–557.
[22] D. Rival, T. Prangemeier, C. Tropea, The influence of airfoil kinematics on the formation of leading-edge vortices in bio-inspired flight, Experiments in Fluids 46 (5) (2009) 823–833.
[23] A. D. Totpal, F. F. Siala, J. A. Liburdy, Energy harvesting of an oscillating foil at low reduced frequencies with rigid and passively deforming leading edge, Journal of Fluids and Structures 82 (2018) 329–342.
[24] J.-C. Lin, D. Rockwell, Force identification by vorticity fields: techniques based on flow imaging, Journal of Fluids and Structures 10 (6) (1996) 663–668.
[25] D. Kim, F. Hussain, M. Gharib, Vortex dynamics of clapping plates, Journal of Fluid Mechanics 714 (2013) 5–23.
[26] J. Li, Z.-N. Wu, Unsteady lift for the wagner problem in the presence of additional leading/trailing edge vortices, Journal of Fluid Mechanics 769 (2015) 182–217.
[27] L. Kang, L. Liu, W. Su, J. Wu, Minimum-domain impulse theory for unsteady aerodynamic force, Physics of Fluids 30 (1) (2018) 016107.

[28] F. F. Siala, M. W. Prier, J. A. Liburdy, Force production mechanisms of a heaving and pitching foil operating in the energy harvesting regime, in: ASME 2018 5th Joint US-European Fluids Engineering Division Summer Meeting, American Society of Mechanical Engineers, 2018, pp. V001T07A002–V001T07A002.
[29] J. Lighthill, Fundamentals concerning wave loading on offshore structures, Journal of Fluid Mechanics 173 (1986) 667–681.
[30] P. G. Saffman, Vortex dynamics, Cambridge university press, 1992.
[31] G. K. Batchelor, An introduction to fluid dynamics, Cambridge university press, 2000.
[32] F. Noca, D. Shiels, D. Jeon, A comparison of methods for evaluating time-dependent fluid dynamic forces on bodies, using only velocity fields and their derivatives, Journal of Fluids and Structures 13 (5) (1999) 551–578.
[33] A. D. Totpal, The energy extraction performance of an oscillating rigid and flexible foil, Ms thesis, Oregon State University, Corvallis, OR (2017).
[34] F. Siala, Experimental and theoretical investigations of the unsteady flow dynamics of oscillating airfoils, PhD dissertation, Oregon State University, Corvallis, OR (2019).
[35] B. Wieneke, Piv uncertainty quantification from correlation statistics, Measurement Science and Technology 26 (7) (2015) 074002.
[36] P. Stevens, H. Babinsky, Experiments to investigate lift production mechanisms on pitching flat plates, Experiments in Fluids 58 (1) (2017) 7.
[37] K. Onoue, K. S. Breuer, Vortex formation and shedding from a cyber-physical pitching plate, Journal of Fluid Mechanics 793 (2016) 229–247.
[38] L. Graftieaux, M. Michard, N. Grosjean, Combining piv, pod and vortex identification algorithms for the study of unsteady turbulent swirling flows, Measurement Science and technology 12 (9) (2001) 1422.